International Journal of Emerging Science and Engineering (IJESE)
ISSN: 2319–6378 (Online), Volume-14 Issue-7, June 2026

Identification of Land Use, Land Cover Change, and Land Surface Temperature (LST) in Ethiopia using Landsat and MODIS Data, East Africa

Agegnehu Kitanbo Yoshe

Abstract: ***This study investigated land use and land cover (LULC) dynamics and their influence on land surface temperature (LST) using multi-temporal Landsat and MODIS satellite imagery. Supervised classification employing the Maximum Likelihood Algorithm was applied to classify LULC patterns, and classification accuracy was assessed following standard validation procedures to ensure reliability for environmental monitoring, water resource management, and climate change assessment. Trend and change detection analyses were conducted to evaluate the spatial and temporal variability of LULC and LST within the study area. The results identified 15 major LULC classes and revealed substantial expansion and contraction among different land cover types over time, accompanied by significant variations in LST. Grassland was the dominant land cover category, accounting for more than 36.53% of the total area. In contrast, the evergreen needle-leaf forest was the least extensive class, covering less than 0.0014% of the study area. The observed changes in LULC and associated thermal characteristics are primarily attributed to both anthropogenic activities and natural environmental processes, which directly influence hydrological conditions, including precipitation, evaporation, streamflow, and water quality dynamics. The findings highlight the strong interrelationship between land-cover transformation and surface thermal responses, emphasising the implications of uncontrolled land-use changes for hydrological balance and ecosystem sustainability. Therefore, the study recommends continuous monitoring and effective management of LULC changes, particularly settlement expansion and deforestation, to mitigate potential environmental degradation and hydrological imbalance within the catchment.***

Keywords: ***Land-Use Change Detections, Land-Surface Temperature Variation, Relationship Between Land-Cover Change And Land-Surface Temperature, Supervised Classification, Landsat and MODIS Datasets, Climatic Change***

Nomenclature:
RS: Remote Sensing
GIS: Geographic Information Systems
LULC: Land Use and Land Cover
NDVI: Normalised Difference Vegetation Index
LST: Land Surface Temperature
USGS: United States Geological Survey
EBFL: Evergreen Broad-Leaf Forest
DBFL: Deciduous Broad-Leaf Forests
ML: Maximum Likelihood
OSL: Open Shrublands
NVM: Natural Vegetation Mosaics
WB: Water Bodies
CSL: Closed Shrublands

Manuscript received on 02 June 2026 | First Revised Manuscript received on 08 June 2026 | Second Revised Manuscript received on 11 June 2026 | Manuscript Accepted on 15 June 2026 | Manuscript published on 30 June 2026.
*Correspondence Author(s)
Dr. Agegnehu Kitanbo Yoshe*, Researcher, Department of Water Resources and Irrigation Engineering, Arba Minch University, 21 Post Office Box, Arba Minch, Ethiopia. Email ID: kitanbo@gmail.com, ORCID ID: 0000-0002-3792-5854

I. INTRODUCTION

Land degradation is a major global environmental challenge driven by rapid population growth, unsustainable land management practices, deforestation, climate change, and other anthropogenic pressures. Currently, Ethiopia has experienced complex changes in land use and land cover (LULC) due to a growing population converting productive agricultural lands to urban areas, a key issue among researchers worldwide [1]. Therefore, in Ethiopia, growing urbanisation and agricultural land use are linked to a growing population, resulting in intensive farming to feed it. Accordingly, many of Ethiopia's major river basins and fertile agricultural lands have become increasingly vulnerable to land degradation, landslides, soil erosion, and declining soil fertility and productivity [2]. Disturbances in land use and land cover (LULC), together with the conversion of natural landscapes into other land-use categories, exert significant impacts on land productivity, river discharge, surface water storage, groundwater recharge and storage, land surface temperature, and geomorphological processes, while also affecting the socio-economic development of the country [3]. The magnitude and nature of these impacts vary considerably across spatial and temporal scales, depending on the intensity, extent, and characteristics of land cover modification and the sensitivity of the surrounding environmental system [4].

Various factors influence land use and land cover (LULC) change, including political conditions, temporal and spatial dynamics, and cultural, economic, and social drivers [5]. LULC change has been widely recognised as a principal driver of environmental transformation, contributing significantly to climate change, biodiversity loss, water resource depletion, soil erosion, and air pollution [6]. These processes alter ecosystem structure and function, disrupt hydrological and biogeochemical cycles, and threaten the sustainability of natural resources and human livelihoods [7]. Consequently, understanding and managing LULC dynamics have become critical priorities for sustainable environmental management, climate adaptation, and long-term socio-economic development [8].

Additionally, variation in land surface temperature is a major driver of land use and land cover. cover change [9]. Changes in land use and land cover contribute to environmental effects [10].

Land surface temperature patterns and their relationship to land use and land cover can provide environmental information to understand climate change [11]. Nowadays, remote sensing and GIS play a significant role in monitoring meteorology [12]. The use of various satellite images assists in analysing and evaluating the effects of LULC change and land surface temperature [13]. Satellite imagery of a specific location at a specific time, mapped using remote sensing and GIS, is used to detect changes in land use, land cover, and land surface temperature [14]. Due to the availability of long-term, high-spatial- and temporal-resolution data and their suitability for various environmental and water resource applications, several recent satellite-based studies have evaluated changes in land use, land cover, and land surface temperature [15]. To the best of the authors' knowledge, comprehensive quantitative analyses of land use and land cover (LULC) dynamics at the national scale remain limited in Ethiopia, despite the country undergoing substantial environmental transformations driven by rapid population growth, urbanisation, industrial expansion, and agricultural intensification [16]. Over recent decades, these processes have significantly altered natural landscapes, hydrological systems, and ecosystem functions across different regions of the country. However, existing studies have largely been conducted at local or regional scales, often lacking integrated nationwide assessments that capture the spatial and temporal complexity of LULC change. Furthermore, considerable gaps remain in the availability of consistent spatial information, long-term environmental datasets, and scientifically grounded analytical frameworks necessary to support evidence-based national planning and sustainable resource management. These limitations constrain the effectiveness of policy formulation, environmental monitoring, and strategic decision-making in land management, water resources, climate adaptation, and ecosystem conservation. Therefore, comprehensive national-scale investigations of LULC dynamics are critically needed to improve understanding of environmental change processes and to support rational planning and sustainable development strategies in Ethiopia.

The main objective of this study is to investigate spatiotemporal changes in land use and land cover (LULC) and land surface temperature (LST) across Ethiopia using multi-source remote sensing datasets. The study aims to assess the interactions between LULC transformation and temperature environmental dynamics to support sustainable economic development, environmental management, and climate change adaptation strategies. The specific objective of this study is to

- To analyses and evaluate spatiotemporal changes in land use and land cover (LULC) classes within the study area using MODIS MCD12Q1 datasets from 2001 to 2022.
- To assess the spatial and temporal variability of land surface temperature (LST) across the study area during the period 2001–2022.
- To evaluate the distribution and variation of land surface temperature associated with each LULC class in the study area.
- To investigate the relationship between LULC transformations and LST dynamics and to determine the influence of land cover changes on surface thermal characteristics between 2001 and 2022.

II. MATERIALS AND METHODS

A. Study Area

Ethiopia is located in Africa between 3° and 15° N and between 33° and 45° E, with an area of 1,129,076.162 square kilometres and a population of 132.67 million in 2024, making it the second most populous country in Africa after Nigeria [17]. The country's climate is primarily governed by altitudinal variation. Conditions are typically torrid and arid at low elevations, whereas the plateau experiences comparatively mild temperatures and higher precipitation. Situated just north of the equator, the country exhibits minimal annual temperature variability; however, markedly cooler conditions prevail in high-altitude mountainous regions [18]. Precipitation is largely controlled by the southwest monsoon, which influences the country from June to September and defines the principal rainy season. In the southeastern region, rainfall is bimodal, with two distinct wet periods: March to May and October to November. In addition, the rainy season is shorter, lasting from February to May in certain areas. Owing to the interplay of multiple atmospheric systems, rainfall demonstrates substantial spatiotemporal variability across individual river basins [19]. A map of the study area is provided in Figure 1 below.

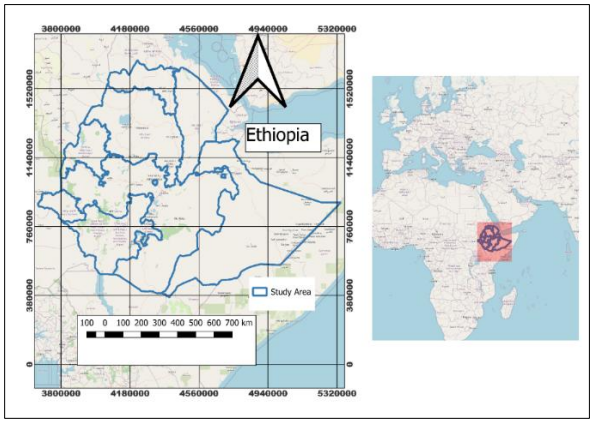

[Fig.1: Location Map of the Study Area Map]

B. Methodology

Land cover detection is a central component of this study, which utilises MODIS datasets spanning 2001–2022 and applies classification schemes consistent with the Ethiopian land use/land cover (LULC) typology. In addition, Landsat imagery from the United States Geological Survey (USGS) portal is used to examine LULC dynamics at a spatiotemporal scale. A supervised classification approach, which is well established in remote sensing applications, is adopted in this study. This method facilitates the categorisation of land-use/land-cover features extracted from satellite imagery. It is based on assigning pixels to predefined classes under the guidance of an image analyst, using algorithmic procedures that link spectral information to specific land cover types. Training sites are selected as representative samples for each identified land-cover class was subsequently used to develop a classification

signature. This signature enables interpretation of spectral characteristics associated with different land-cover categories, thereby allowing systematic classification of remotely sensed data [20]. Among supervised classification algorithms, the Maximum Likelihood (ML) classifier is one of the most widely applied techniques for image classification. This method is grounded in probability theory and assumes that the training data for each land cover class, across all spectral bands, follow a normal (Gaussian) distribution [21]. Furthermore, MODIS datasets are utilised to derive additional biophysical variables, including land surface temperature (LST) and evapotranspiration. Both LULC and LST analyses are conducted over a two-decade period (2001–2022), with thematic maps generated for the years 2001, 2006, 2011, 2017, and 2022 to capture temporal dynamics. All image processing, classification, and spatial analyses are performed using ArcMap 10.4 software. Thematic map production and areal computations are likewise conducted within this environment. The overall methodological workflow is summarised in Figure 2 as a flowchart.

i. Data Acquisition

Remotely sensed and spatial datasets are widely recognised as reliable sources for analysing and interpreting land use and land cover (LULC) dynamics across diverse landscapes [29]. Remote sensing involves acquiring information about the Earth's surface without direct physical contact, typically via satellites, aircraft, drones, or ground-based sensors that capture multispectral imagery and related geospatial data. The choice of platform is determined by the required spatial and spectral resolution, with satellites commonly used for large-scale mapping and drones for high-resolution, site-specific analysis. Both active (energy-emitting) and passive (energy-detecting) sensing systems are employed depending on the application. For this study, cloud-free remotely sensed imagery was prioritised to improve classification accuracy. Image pre-processing included noise reduction, geometric and radiometric correction, and feature enhancement prior to classification. Specifically, MODIS Land Cover Type Version 6.1 (MCD12Q1 V6.1) data from NASA's LP DAAC archive, accessed via the USGS Earth Explorer platform (https://earthexplorer.usgs.gov, accessed on 25 July 2024), were utilised for LULC classification. Data obtained from USGS Earth Explorer provides freely available satellite imagery; however, due to the limited availability of cloud-free scenes, a maximum cloud cover threshold of 10% was applied, resulting in datasets with approximately 4–6% cloud cover, which did not significantly affect classification accuracy. The datasets, downloaded in HDF format, were processed in ArcGIS 10.4. To minimise seasonal bias in vegetation dynamics and LULC change detection, imagery from comparable seasonal periods was used [22].

ii. Pre- Processing Data

Publicly available remote sensing datasets are not inherently error-free; therefore, rigorous pre-processing is essential to minimise noise, ensure data consistency, and enhance suitability for subsequent analyses. Such procedures improve both visual interpretability and spectral separability of land surface features, while also providing higher-quality inputs for automated image classification algorithms. In this study, all preprocessing was conducted using ArcGIS 10.4. The workflow included georeferencing, radiometric and geometric correction, band compositing (layer stacking), mosaicking, band extraction, and spatial clipping prior to classification. These steps produced radiometrically and geometrically corrected satellite datasets—geometric corrections involved reprojecting and resampling all datasets to the Adindan_UTM_Zone_37N coordinate system (Transverse Mercator projection). Radiometric normalisation was applied to ensure comparability across multi-temporal images for time-series analysis. Individual spectral bands were extracted using the ArcGIS Spatial Analyst extension. Following mosaicking, the datasets were clipped to the study area boundary using standard raster processing tools within ArcGIS 10.4.

iii. Image Classification

An appropriate classification framework is fundamental to the accurate interpretation of satellite imagery in the study area; accordingly, a modified classification scheme was adopted to delineate LULC categories. Per-pixel supervised classification was employed, whereby image pixels are assigned to classes based on similar spectral reflectance characteristics [34]. For the 2001–2022 dataset, a Maximum Likelihood Classification (MLC) algorithm implemented in ArcGIS 10.4 was used to derive land-use and land-cover information. The classification procedure comprised three main stages: training, sample selection, and classification, followed by accuracy assessment. Initially, an "interpretation key" representing the spectral signatures of each land cover class was developed using representative training sites. Approximately 300 training samples were generated for each class to ensure statistical robustness. Each pixel was then probabilistically assigned to the class to which it most closely corresponds. The Maximum Likelihood method, one of the most widely applied parametric classifiers in LULC studies, assumes that the probability distribution of each class follows a multivariate normal distribution and assigns pixels based on Bayesian probability principles. Specifically, classification is determined by estimating the likelihood that an observation vector X belongs to a given class Mc using Bayesian decision rules (Equation 1).

$$d = \ln(ac) - [0.5 * \ln(|covc|)] - [0.5 * (X - M_c) * T * (covc^{-1}) * (X - M_c)] \quad (1)$$

Where c is a specific class; d is weighted distance (likelihood); X is the candidate pixel's measurement vector; Mc is the sample's mean vector; and ac is the likelihood in percent that any candidate pixel belongs to class C (defaults to 1.0, or is entered from a priori knowledge); Covc is the covariance matrix for the class c pixels in the sample; |Covc| is its determinant in matrix algebra, Covc− 1 is its inverse, ln is its natural logarithm function, and T is its transposition function (matrix algebra). In the classification approach, eight major land-use/land-cover classes were developed, including savannas, grasslands, evergreen broadleaf forests, permanent wetlands, croplands, vegetation mosaics, water bodies, and barren ground.

iv. Accuracy Assessment

Following completion of the land use/land cover (LULC)

Published By:
Blue Eyes Intelligence Engineering
and Sciences Publication (BEIESP)

classification process, spatially explicit LULC datasets covering 2001 to 2022 were generated to analyse temporal and spatial patterns of land cover dynamics within the study area. To ensure the reliability and validity of the classified outputs, a comprehensive accuracy assessment was conducted by comparing the classified LULC categories with corresponding reference data derived from ground truth information, high-resolution imagery, and ancillary spatial datasets. The accuracy evaluation focused on the classified LULC maps for 2001, 2011, and 2022, selected to represent key temporal intervals within the study period. The assessment was performed using a confusion matrix (error matrix), which provides a statistical comparison between classified data and reference observations. Based on this matrix, standard accuracy indicators were computed, including producer's accuracy, user's accuracy, overall classification accuracy, and the Kappa coefficient. The producer's accuracy was used to evaluate the probability that a reference land cover class was correctly classified in the generated map, thereby indicating omission errors. The user's accuracy measured the reliability of the classified categories from the perspective of map users and reflected commission errors. Overall accuracy represented the proportion of correctly classified samples relative to the total number of reference samples. In addition, the Kappa coefficient was used to quantify the degree of agreement between the classified maps and the reference data while accounting for chance agreement. These statistical measures provided a robust evaluation of the classification performance and the reliability of the generated LULC maps, as expressed in Equation (2).

$$OA = \frac{\text{Total correctly classified pixels}}{\text{Total of classified pixels}} * 100 \qquad (2)$$

Overall accuracy (OA) is calculated by dividing the total number of correctly classified pixels (i.e., the sum of the major diagonal) by the total number of reference pixels.

$$PA = \frac{\text{Number of correctly classified pixels per class}}{\text{Number of reference totals per class}} * 100 \qquad (3)$$

The producer's accuracy (PA) indicates how well test set pixels of the given cover type are classified.

$$UA = \frac{Number\ of\ correctly\ classified\ pixels\ per\ class}{Number\ of\ classified\ totals\ per\ class} * 100 \quad (4)$$

The user's accuracy (UA) is a measure of commission error that indicates the probability that a pixel classified into a given category actually represents that category on the ground.

$$K_{stat} = \frac{N\sum_{i=1}^{r} X_{ij} - \sum_{i=1}^{r}(X_{RT} - X_{CT})}{N^2 - \sum_{i=1}^{r}(X_{RT} - X_{CT})} \qquad (5)$$

Where Kstat is the Kappa statistic, N is the total number of samples, Xij is the product of the total number of samples and total diagonal values, XRT is the row total, XCT is the column total, and r is the number of categories. Statistics or coefficients evaluate the difference between the actual agreement of a classified map and the chance agreement of a random classifier, relative to reference data [23].

v. Change Detection

Owing to their cost-effectiveness, extensive spatial coverage, and high temporal resolution, remote sensing and GIS-based techniques are extensively utilised for land use/land cover (LULC) change detection. Multi-temporal remotely sensed datasets facilitate inter-temporal analysis by enabling the identification and quantification of spatial changes over time. Among the available approaches, post-classification comparison is one of the most widely adopted methods for LULC change analysis. This technique involves independently classifying satellite images acquired at different time periods, followed by a class-by-class comparison to detect and quantify changes in land-cover categories. Previous studies have demonstrated that post-classification comparison provides relatively high classification accuracy and reliable change detection performance compared with other analytical techniques [24, 25].

In this study, land use/land cover (LULC) changes in Ethiopia were assessed using a post-classification comparison approach based on the Maximum Likelihood Classification (MLC) of Landsat imagery. Following classification, raster outputs were converted into vector format to facilitate spatial analysis and quantitative assessment of LULC transitions. Changes within each land cover category were subsequently quantified and mapped independently to enhance interpretability and support detailed spatial evaluation. The accuracy and reliability of the change detection results are inherently dependent on the quality and precision of the underlying classified thematic maps [23,26]. Accordingly, the magnitude of change (C) for each LULC category between 2001 and 2022 was computed using the following equation.

$$C_{ij} = X_j - X_i \qquad (6)$$

Where Xi is the initial year of the LULC area, Xj is the final year of the LULC area, and Cij is the change in LULC class (the total gain or loss of LULCC).

The change in class is divided by the covered area in the base year, then multiplied by 100. A straightforward computation was used to calculate the percentage change (C%). And it has been conducted in each land-use class [23, 26].

$$P_{ij} = \frac{C_{ij}}{X_i} * 100 \qquad (7)$$

IJ indicates the number of classes in the image. Cij indicates how much class IJ has changed. (Pij) is the percentage change in class IJ. Xi is "basic image" (20001). The most current picture is Xj (2022).

vi. Land Surface Temperature

Variation in land surface temperature (LST) represents a critical factor influencing land use and land cover (LULC) dynamics. In this study, monthly daytime LST data derived from MODIS terrestrial emissivity products were obtained from the NASA Earthdata portal. for the period 2001–2022 to evaluate long-term temperature variability.

Monthly datasets with a spatial resolution of 0.05° were selected due to their superior spatiotemporal consistency compared with daily 1 km products [27,28]. The daytime MODIS LST datasets were processed in ArcGIS 10.4 and clipped to the study area boundary. To generate spatial LST maps, raster data were converted into point features, and temperature values were extracted for each point. The extracted values were multiplied by the MODIS scale factor (0.02) and subsequently converted from Kelvin to degrees Celsius by subtracting 273.15. Annual and seasonal LST patterns, as well as interannual variability, were then analysed. It should be noted that MODIS-derived LST values may differ from ground-observed temperatures due to atmospheric conditions, particularly cloud cover, which can influence satellite-based thermal measurements [28].

vii. Land Surface Temperature Extraction from Thermal Band

- **Conversion of the Digital Number(DN) to Spectral Radiance($L\lambda$)**

All objects emit thermal electromagnetic radiation when their temperature is above absolute zero (0 K). Based on this principle, signals recorded by thermal remote sensing sensors can be converted into at-sensor spectral radiance. Accordingly, the spectral radiance was computed using Equation (8), following the Landsat Project Science Office (2002) formulation.

$$L\lambda =' gain' * qcal + 'offset' \qquad (8)$$

Where gain is the slope of the radiance/DN conversion function; DN is the digital number of a given pixel; bias is the intercept of the radiance/DN conversion function. This is also given as:

$$L\lambda = lmin\lambda + [(lmax\lambda - lmin\lambda)/(qcalmax - qcalmin) * qcal] \qquad (9)$$

Where qcalmin = 0, qcalmax = 255 and qcal is the digital number of each pixel. They are the spectral radiance for band 6 at digital numbers 0-255, respectively. These compute to 3.2 W ·m2· sr and 12.65 W · m2 · sr, respectively. Equation 9 was substituted with the respective values and simplified to equation 10.

$$L\lambda = (0.037059 * DN) + 3.2 \qquad (10)$$

- **Conversion of Spectral Radiance to At-Satellite Brightness Temperature(TB)**

Corrections for emissivity (e) have been applied to the radiant temperatures based on the nature of the land cover. Generally, vegetated areas are given a value of 0.95 and non-vegetated areas 0.9-2. Artis and Carnahan have computed the emissivity-corrected surface temperature [44].

$$TB = \frac{K_2}{\ln\left(\frac{K_1}{L_\lambda}+1\right)} \qquad (11)$$

where: TB = At-satellite brightness temperature (K) $L\lambda$ = Spectral Radiance in W.m2 .sr1 .lm1 K1 and K2 = K2 and K1 are two pre-launch calibration constants. (For the Landsat 7 ETM+6.2 band, these compute to 1282.71 K and 666.09 W.m2 .sr1 .lm, respectively).

viii. Land Surface Temperature(LST)

The derived temperature values are referenced to a blackbody assumption; therefore, an emissivity (ε) correction is required to obtain physically realistic land surface temperature estimates. This correction can be implemented either by assigning emissivity values based on land-cover type [45] or by estimating pixel-specific emissivity from the Normalised Difference Vegetation Index (NDVI). In this study, emissivity-adjusted land surface temperature (LST) was computed using the formulation proposed by Artis and Carnahan [44], as presented in Equation (12).

$$ST = \frac{T_B}{\left[1+\{\left(\lambda*\frac{TB}{\rho}\right)*ln\varepsilon\}\right]} \qquad (12)$$

Where ST = land surface temperature in Kelvin, λ = wavelength of emitted radiance in meters (for which the peak response and the average of the limiting wavelengths (λ = 11.5 lm) [Markham and Barker, 1985] is used, ρ = h * c/ ρ (1.438 * 102 m K), ρ = Boltzmann constant (1.38 * 1023 J/K), h = Planck's constant (6.626 * 1034 J s), and c = velocity of light (2.998 * 108 m/s) and Ɛ = emissivity (ranges between 0.97 and 0.99), see equation 13

$$\text{land surface emissivity } (\varepsilon) = 0.004*Pv + 0.986 \qquad (13)$$

For NDVI extraction, the method of Townshend and Justice [46, 47] was applied.

$$NDVI = \frac{IR_{band}-R_{band}}{IR_{band}+R_{band}} \qquad (14)$$

where IR = near infrared band (band 4 of MSS and TM), R = red band (MSS band 2, TM band 3)

whereas the proportion of vegetation (Pv) can be calculated as Eq. 15

$$P_v = \left(\frac{NDVI_{jr}-NDVI_{min}}{NDVI_{max}-NDVI_{min}}\right)^2 \qquad (15)$$

C. Conversion of LST from Kelvin to Degrees Celsius

For ease of comprehension, the above-derived LST units were converted to degrees Celsius using the relation 0 °C = 273.15 K. The workflow of the methodology is shown in Figure 2 below.

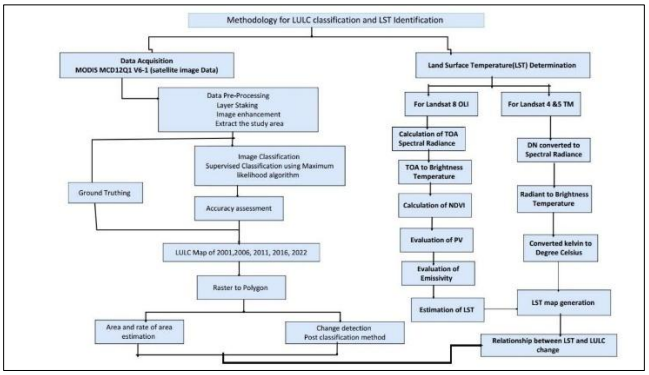

[Fig.2: Flow Chart of the Methodology]

III. RESULT AND DISCUSSION

A. Accuracy Assessment of the LULC Classification

Based on the evaluation, the results showed that the overall accuracy and kappa statistics for all land-use types in Ethiopia were acceptable across the study. periods of 2001, 2006, 2011, 2016 and 2022 (Table I). In the present research, the

Published By:
Blue Eyes Intelligence Engineering
and Sciences Publication (BEIESP)

classification accuracy met the criterion of at least 80% for sensor data. For each LULC classification, an accuracy assessment was calculated from 2001 to 2022, and the results demonstrate that user accuracy ranged from 95.6% to 98.4%. The producer accuracy of the LULC classification ranges from 93.8% to 98.2%, indicating well-classified LULC maps and being within the range for further analysis. The Kappa coefficient values indicate strong agreement, ranging from good to very good according to the classification criteria adopted by Aliani et al. [29]. As shown in Table I, Kappa values ranged from 0.86 to 0.95, corresponding to substantial to near-perfect agreement as defined in previous studies. In addition, the overall classification accuracy ranged from 94.6% to 98.4% (Table I), reflecting a high level of reliability. These results demonstrate that the generated LULC maps are sufficiently accurate for robust analysis of land-use and land-cover change dynamics, consistent with findings reported in similar studies. The combined assessment of user accuracy, producer accuracy, overall accuracy, and the Kappa coefficient (Table I.) further highlights the strong performance of the classification approach in integrating remote sensing-derived indices for multi-temporal LULC mapping. Accordingly, these methods are considered reliable and appropriate for subsequent applications, including modelling future LULC scenarios [30]. Overall, the classified outputs are deemed valid for evaluating LULC change dynamics within the study area and agree with other similar studies [31].

Table I: Accuracy Assessments of the Land Use/Land Cover Class

	2001	2006	2011	2016	2022
User accuracy	96.8	95.6	98.2	96.5	98.4
Producer's accuracy	95.0	98.2	97.9	94.5	93.8
Kappa coefficient	0.86	0.88	0.95	0.94	0.92
Overall accuracy	97.3	98.4	94.6	95.5	94.8

B. Change in Land Use/Land Cover Between 2001 and 2022 from MODIS

In this study, a supervised classification approach based on the Maximum Likelihood algorithm was applied to MODIS and Landsat imagery. Based on dominant land use/land cover (LULC) characteristics, the study area was classified into the following categories: evergreen needle-leaf forest (ENFL), evergreen broad-leaf forest (EBFL), deciduous broad-leaf forest (DBFL), mixed forest (MFL), closed shrubland (CSL), open shrubland (OSL), woody savanna (WSL), savanna (SL), grassland (GL), permanent wetland (PWL), cropland (CL), urban and built-up land (BUL), natural vegetation mosaic (NVM), barren land (BL), and water bodies (WB). Based on the results obtained, the dominant LULC was grassland, covering 36.53-44.75% during the study period. In contrast, evergreen needle-leaf forest land use/land cover was the lowest, with an area coverage of less than or equal to 0.0014%. The second dominant LULC was savanna land, covering an area between 15.92% and 17.56 % during the study period. The calculated land use and land cover classification for the study period from 2001 to 2022 shows gains and losses in the area coverage of LULC classes. The ENFL, WSL, GL and BUL show increasing trends during the study period. EBFL, MFL, CSL, OSL and NVM show decreasing trends. Higher variation in the increasing and decreasing trends of DBFL, SL, PWL, CL, and BL was observed during the study period. The highest ENFL area coverage was observed in 2018 with an area of 17.9 km². For the selected years, the area percentage of ENFLs increased from 0.0003% (2001) to 0.0014% (2022), respectively. The EBFL has been reduced from 2.48% (2001) to 2.05% (2021) and increased to 2.16% (2022). The DBFL has been reduced from 0.94% (2001) to 0.44% (2016) and increased to 0.66% (2022). The MFL has been reduced from 0.05% (2001) to 0.01% (2022). The CSL has been reduced from 3.49% (2001) to 1.93% (2022). The OSL is falling and rising, from 18% (2001) to 13.07% (2006), 14.99% (2011), 13.51% (2016), and 14.96% (2022). The WSL has increased from 0.38% (2001) to 1.01% (2022). The SL has been reduced from 17.56% (2001) to 15.92% (2002). The GL shows an increasing trend from 36.53% (2001) to 42.91% (2006), then a decreasing trend to 41.95% (2011), 43.24% (2016), and 42.38% (2022). The PWL shows a decrease, then an increase, from 0.1% (2001) to 0.05% (2006), 0.08% (2016), and 0.12% (2022). The CL shows have been reduced from 14.11% (2001) to 13.77% (2006) and increased to 14.97% (2022). The BUL increased from 0.12% (2001) to 0.13% (2022). The NVM has been reduced from 0.69% (2001) to 0.19%(2022).

The BL shows an increasing trend from 4.91% (2001) to 5.1% (2006), 5.29% (2011), 5.24% (2016), and 4.9% (2022), then a decreasing trend. The WB shows decreasing and increasing trends from 0.65% (2001) to 0.61% (2016) and to 0.65% (2022). The total area of the study was 1129071 km². The areas of the ENFL were 3.75, 3.97, 8.42, 16.16, and 15.81 km² in 2001, 2006, 2011, and 2022, respectively. The detailed analysis of the remaining LULC classes is presented in Table II. The spatial distribution of land use/land cover (LULC) exhibits substantial variation across the selected years (2001–2022), reflecting pronounced gains and losses among LULC classes over the study period, as shown in Figure 3. The resulting analyses provide critical spatial information with direct relevance for policy formulation and decision-making processes. These findings enable stakeholders to evaluate the effectiveness of existing land-use policies critically, anticipate emerging environmental and socio-economic challenges, and develop appropriate adaptive strategies. Furthermore, the integration of spatially explicit change patterns and scenario-based insights supports evidence-informed decision-making to promote sustainable development, improved natural resource management, and long-term socio-economic resilience.

Table II: Percentage of Area Under Different LULC Classes in Different Time Periods from 2001 to 2022

Type of LULC	2001		2006		2011		2016		2022	
	Area									
	Km²	%	Km²	%	Km²	%	Km²	%	Km²	%
ENFL	3.75	0.0003	3.97	0.0004	8.42	0.0007	16.16	0.0014	15.81	0.0014
EBFL	27979.34	2.48	26470.36	2.34	24588.74	2.18	23202.07	2.05	24428.07	2.16
DBFL	10576.07	0.94	7112.96	0.63	5366.86	0.48	4984.66	0.44	7484.29	0.66
MFL	550.32	0.05	212.17	0.02	120.81	0.01	90.90	0.01	80.97	0.01
CSL	39428.83	3.49	34710.18	3.07	29768.62	2.64	29050.55	2.57	21791.74	1.93
OSL	203271.71	18.00	147518.61	13.07	169233.93	14.99	152505.15	13.51	168945.53	14.96
WSL	4258.64	0.38	7670.13	0.68	10030.66	0.89	11144.47	0.99	11435.42	1.01
SL	198240.69	17.56	196080.24	17.37	186374.96	16.51	183906.13	16.29	179793.04	15.92
GL	412399.40	36.53	484455.93	42.91	473632.82	41.95	488261.45	43.24	478516.48	42.38
PWL	1155.85	0.10	518.82	0.05	607.25	0.05	930.22	0.08	1317.65	0.12
CL	159319.77	14.11	155515.64	13.77	158270.87	14.02	164402.60	14.56	169073.47	14.97
BUL	1361.85	0.12	1370.71	0.12	1384.22	0.12	1398.61	0.12	1437.13	0.13
NVM	7808.10	0.69	2991.48	0.26	3010.56	0.27	3204.11	0.28	2133.99	0.19
BL	55424.11	4.91	57608.10	5.10	59714.53	5.29	59136.76	5.24	55270.82	4.90
WB	7292.73	0.65	6838.30	0.61	6960.97	0.62	6836.55	0.61	7351.74	0.65

Figure 3 illustrates the spatial distribution of land use and land cover (LULC) across the study area, revealing a marked heterogeneity in the distribution of dominant land cover types. Cropland is the predominant class in central Ethiopia, particularly concentrated in the central and northern parts of the region. In contrast, grassland is relatively widespread across the study area, though its presence is more limited in the eastern and southeastern zones. Open shrubland is the dominant land cover type in the southwestern part of the study area, whereas savanna is more prevalent in the western regions. These spatial patterns indicate pronounced intra-regional variability in LULC composition and structure. Furthermore, vegetation distribution, density, and spatial continuity play a critical role in regulating land surface temperature (LST) across the landscape, thereby influencing local and regional thermal conditions.

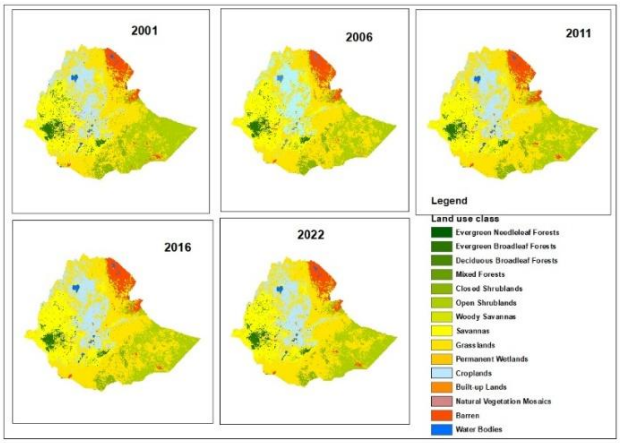

[Fig.3: Land use Land Cover Classes from 2001-2022 for the Study Area]

C. Change Detection Analysis

The change detection analysis was conducted to examine in greater detail the spatial and areal transitions among land use/land cover (LULC) classes across the selected temporal intervals. This analysis facilitates systematic quantification of land cover dynamics, enabling identification of gains and losses within individual LULC categories over time. The resulting change matrices and corresponding statistical summaries are presented in Table III. The results show that the FNFL increased by 5.88% (0.22 km²) between 2001 and 2006, by 118.47% (4.45 km²) between 2006 and 2011, by 206.17% (7.74 km²) between 2011 and 2016, and decreased by 9.33% (-0.35 km²) between 2016 and 2022. EBFL decreased by 5.39% (-1508.89 km²), 6.73% (1881.62 km²), and 4.96% (-1386.66 km²) between 2001 and 2006, 2006 and 2011, and 2011 and 2016, respectively, whereas between 2016 and 2022 it increased by 4.38% (1226 km²). MFL shows decreasing trend by 61.45%(-338.15 km2), 16.6%(-91.36km2), 5.43%(-29.91km2) and 1.8%(9.93km2), CSL by 11.97(-4718.64km2), 12.53%(-4941.56km2), 1.82%(-718.07km2) and 18.41%(-7258.81), SL by 1.09%(-2160.45km2), 4.9%(-10823.11km2), 1.25%(-2468.83km2) and by 2.07%(-4113.09km2) between 2001-2006, 2006-2011, 2011-2016, and 2016-2022 respectively, whereas WSL was increased by 80.11%(3411.49km2), 55.43(2360.52km2), 26.15%(1113.81km2) and 6.83%(290.96km2), BUL by 0.65%(8.86km2), 0.99%(13.51km2), 1.06%(14.39km2) and by 2.83%(38.51km2) between 2001-2006, 2006-2011, 2011-2016, and 2016-2022 respectively. A detailed assessment of the rate of land use/land cover (LULC) change, including class-specific transitions and areal shifts among categories, is presented in Table III. Overall, notable variations in LULC were observed across the study periods, particularly between 2001–2006, 2006–2011, 2011–2016, and 2016–2022. Change detection was implemented through a post-classification cross-tabulation of image pairs from successive time periods, enabling both qualitative identification of transition pathways and quantitative estimation of land-cover dynamics over the full study period (2001–2022). The resulting analysis provides detailed areal statistics, including net changes for each LULC class, expressed as gains (positive values in area or percentage) and losses (negative values), thereby capturing the magnitude and direction of landscape transformation. Overall, the observed LULC transitions indicate substantial land-system reorganisation over time, with important implications for local climatic conditions. In particular, the reduction in vegetated and green land cover is likely to exacerbate surface thermal conditions, thereby increasing land surface temperature and associated environmental stress within the study area.

Table III: Change of Land Use and Land Cover for the Study Area Between 2001-2006, 2006-2011, 2011-2016, and 2016-2022

LULC class	Change of LULC class							
	2001&2006		2006&2011		2011&2016		2016&2022	
	area in Km²	%	area in Km²	%	area in Km²	%	area in Km²	%
ENFL	0.22	5.88	4.45	118.47	7.74	206.17	-0.35	-9.33
EBFL	-1508.98	-5.39	-1881.62	-6.73	-1386.66	-4.96	1226.00	4.38
DBFL	-3463.10	-32.74	-1746.11	-16.51	-382.19	-3.61	2499.63	23.63
MFL	-338.15	-61.45	-91.36	-16.60	-29.91	-5.43	-9.93	-1.80
CSL	-4718.64	-11.97	-4941.56	-12.53	-718.07	-1.82	-7258.81	-18.41
OSL	-55753.10	-27.43	21715.32	10.68	-16728.77	-8.23	16440.38	8.09
WSL	3411.49	80.11	2360.52	55.43	1113.81	26.15	290.96	6.83
SL	-2160.45	-1.09	-9705.28	-4.90	-2468.83	-1.25	-4113.09	-2.07
GL	72056.54	17.47	-10823.11	-2.62	14628.63	3.55	-9744.97	-2.36
PWL	-637.03	-55.11	88.43	7.65	322.96	27.94	387.43	33.52
CL	-3804.13	-2.39	2755.23	1.73	6131.73	3.85	4670.88	2.93
BUL	8.86	0.65	13.51	0.99	14.39	1.06	38.51	2.83
NVM	-4816.62	-61.69	19.08	0.24	193.55	2.48	-1070.13	-13.71
BL	2183.99	3.94	2106.43	3.80	-577.77	-1.04	-3865.94	-6.98
WB	-454.43	-6.23	122.67	1.68	-124.42	-1.71	515.19	7.06

D. The Spatio-Temporal Pattern of NDVI for the Study Area

Figure 4 shows the spatial distribution of the evaluated NDVI for the study area in 2001, 2006, 2011, 2016, and 2022. From Table IV, the mean NDVI values for the study area were 0.32 in 2001, 0.29 in 2006, 0.3 in 2011, 0.34 in 2016, and 0.32 in 2022. This index shows vegetation health, stress, and greenness (biomass) in the study area, consistent with similar studies. According to Sahana, Ahmed, and Sajjad, NDVI values greater than 0.3 indicate healthy vegetation. As presented in Figure 4, the green-colored area shows healthy vegetation having an NDVI of more than 0.3, and the red-colored area shows trees having an NDVI of less than 0.3. The standard deviations of NDVI were 0.15, 0.26, 0.28, 0.29, and 0.31 in 2001, 2006, 2011, 2016, and 2022, respectively. The evaluated vegetation production values were 0.2318, 0.0020, 0.0021, 0.0027, and 0.0024 for 2001, 2006, 2011, 2016, and 2022, respectively, whereas the land surface emissivity of the study area was 0.9 for the study period. The estimated mean land surface temperatures for the study area are 34.7, 33.5, 34.4, 34.67, and 34°C, with standard deviations of 6.21, 5.86, 5.7, 6, and 5.8 in 2001, 2006, 2011, 2016, and 2022, respectively. The Normalised Difference Vegetation Index (NDVI) exhibits a strong and consistent relationship with the spatial variability of land surface temperature (LST), thereby providing a robust means of validating LST heterogeneity, consistent with previous studies [32]. Areas characterised by higher NDVI values are generally associated with lower surface temperatures. In contrast, regions with low vegetation density are associated with significantly elevated LST values, as shown in Figures 4 and 5. Over the study period (2001–2022), NDVI values exhibit both increasing and decreasing trends, closely mirrored by corresponding variations in mean LST, indicating a coherent but inverse vegetation–temperature relationship. The statistical analysis reveals a strong negative correlation between NDVI and LST, with a correlation coefficient of 0.95, indicating a highly significant relationship consistent with findings reported by Chen and Zhang [33]. Similarly, Guha and Govil [34] identified a strong association between vegetation cover and surface temperature dynamics. These results are further supported by Rosca et al. [35], who emphasised that the NDVI–LST relationship is particularly pronounced in areas with sparse vegetation cover. Overall, the observed findings demonstrate strong agreement with a broad body of literature spanning diverse geographic and climatic settings [36-39], thereby confirming the robustness and generalisability of the vegetation–temperature linkage.

Table IV: NDVI and Land Surface Temperature for the Study Area from 2001 to 2022

	NDVI				Temperature			
Year	Max	Min	Aveg	St.D	Max	Min	aveg	St. D
2001	0.88	-0.20	0.32	0.15	56.4	11.8	34.7	6.21
2006	0.95	$4.3x10^{-5}$	0.29	0.26	53.8	10.1	33.5	5.86
2011	0.97	$1.5x10^{-5}$	0.3	0.28	53.87	12.73	34.4	5.7
2016	0.79	$9.6x10^{-5}$	0.34	0.29	55.64	11.8	34.67	6
2022	0.75	$5.75x10^{-5}$	0.32	0.31	53.68	12.16	34	5.8

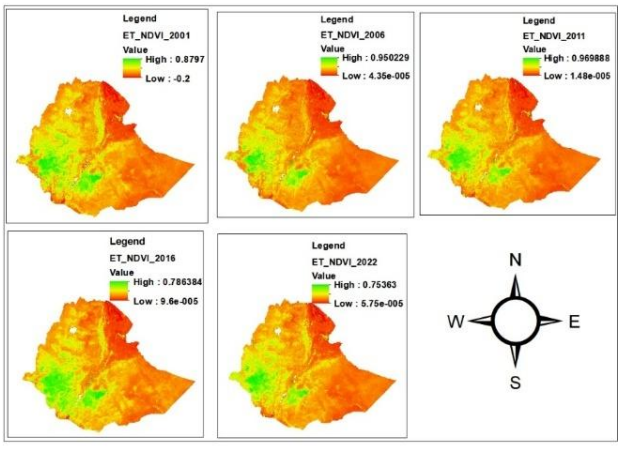

[Fig.4: Spatial Variation of NDVI for the Study Area From 2001-2022]

E. Land Surface Temperature (LST)

Figure 5 indicates the evaluated spatial distribution of land surface temperature during study periods in 2001, 2006, 2011, 2016 and 2022 for the

Published By:
Blue Eyes Intelligence Engineering
and Sciences Publication (BEIESP)

study area. The blue colour indicates the highest temperature, whereas the red colour indicates the lowest temperature. The results show that the minimum and maximum land surface temperatures in the study area range from 11.8 to 56.4°C in 2001, with an average of 34.7°C. The mean spatial distribution of the study area LST ranges from 11.8 to 56.4°C in 2001, from 10.1 to 53.8°C in 2006, from 12.7 to 53.9°C in 2011, from 11.8 to 55.6°C in 2016, and from 12.2 to 53.7°C in 2022. The figure presents varying trends from 2001 to 2022. The drought, as a natural phenomenon, was a key driver of variability in land surface temperature. However, other climatic factors, such as wind speed, also influence land surface temperature, as reported in similar studies [40]. The highest land surface temperature was in the northwestern part of the study area, and the lowest was in the central part. The mean yearly temporal variation of land surface temperature for the selected years is 34.7, 33.5, 34.4, 34.67 and 34°C in 2001, 2006, 2011, 2016 and 2022, respectively. Variability in land-use and land-cover classes also affects the land surface temperature in the study area. In general, the highest land surface temperatures were observed in areas with bare soil, and the lowest in forests and high mountains.

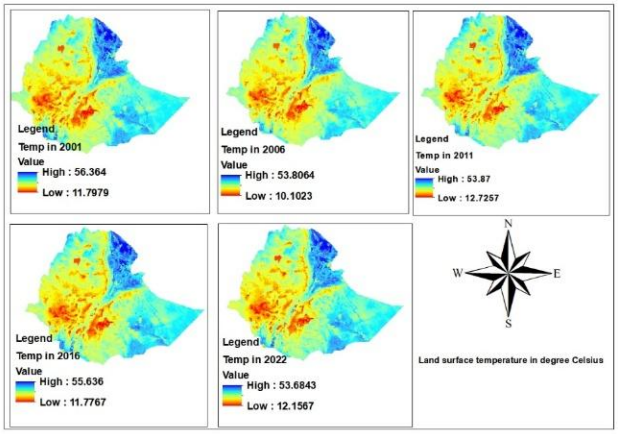

[Fig.5: Spatial Distribution of Land Surface Temperature in the Study Area from 2001-2022]

F. Temperature Variations for Different Land Cover Types

Remotely sensed land surface temperature (LST) represents the radiative energy emitted from the Earth's surface, encompassing a range of land cover types, including building rooftops, impervious and paved surfaces, vegetation, bare soil, water bodies, and grasslands. As such, LST serves as an integrated indicator of surface energy balance and is highly sensitive to variations in land use and land cover (LULC). Table V presents the mean LST values for different LULC categories across the study area during 2001–2022. The results highlight clear thermal heterogeneity among land cover classes, reflecting the influence of surface composition and land management practices on the spatial distribution of temperature. In this context, Landsat satellite imagery provides a valuable dataset for examining LULC dynamics and for assessing their corresponding impacts on LST variability across different land cover types. It is found from the result that the highest temperature was observed on barren land with the value of 55.64°C in 2016, whereas the lowest temperature was observed in the EBFL in 2001 with the value of 10.1°C. Figure 6 demonstrates the dominant land-use/land-cover with land surface temperature. It demonstrates that the average land surface temperature was 20.8, 21.45, 18.3, 18.4 OC and 19.14 OC for ENFL, 23, 22.6, 23.3, 23.4 OC and 22.72 OC for EBFL, 30.1, 28.84, 29.44, 29.56 and 28.3OC for DBFL, 27, 27.03, 27.31, 26.62 OC and 26.21 OC for MFL, 33.9, 32.6, 34.53, 34.31 OC and 34.8OC for CSL, 39.9, 38.4, 39.25, 39.9 OC and 39 OC for OSL, 23.1, 22.96, 23.9, 23.9 and 23.6 OC for WSL, 29.8, 29.24, 29.9, 29.86 and 29OC for SL, 35.4, 34.2, 35.1, 35.6 OC and 35 OC for GL, 27.14, 26.6, 26.42, 27.65 OC and 26.7OC for PWL, 32.17, 31.2, 31.8, 31.7 and 31.17 OC for CL, 34.66, 33.15, 34.22, 33.93 OC and 33.61 OC for BUL, 26.33, 25.4, 26.1, 25.86 and 25.63 OC for NVM, 45.54, 44.15, 43.95, 45.1 OC and 43.92 OC for BL and 25.8, 25.5, 25.55, 25.84 OC and 25.1 OC in 2001, 2006, 2011, 2016 and 2022 respectively. For the calculated land surface temperature, the maximum temperature was observed in open shrublands, grasslands, built-up lands and barrens for each year. From the observed maximum temperatures, the highest temperature was on barren land in 2016, with values of 56.4, 53.81, 53.9, 55.64, and 53.68°C in 2001, 2006, 2011, 2016, and 2022, respectively. In contrast, the minimum temperature was 10.1°C, observed in evergreen needleleaf forests and evergreen broadleaf forests. This variation in land surface temperature is due to vegetation cover, which affects land surface evapotranspiration and emissivity, consistent with other studies [41]. In addition, Tan et al. [42] demonstrated that land surface temperature (LST) varies significantly across different land use/land cover (LULC) categories, highlighting the strong influence of surface characteristics on thermal conditions. More recently, Mustafa et al. [43] reported an increasing trend in LST driven by land-use change and rising population density in Beijing, China, a finding consistent with the results of the present study. It is also important to note that areas exhibiting no apparent changes in land use and land cover still display spatial variability in surface temperature, indicating the influence of additional controlling factors beyond LULC dynamics. In particular, broader climatic processes, including regional climate change, play a significant role in modulating LST, especially in arid and semi-arid environments, where these changes may intensify drought and exacerbate thermal stress. Overall, the results of this study indicate pronounced spatial and temporal variability in land surface temperature across the study area during 2001–2022, reflecting the combined influence of land-cover characteristics and broader climatic drivers. The standard deviation of land surface temperature for ENFL ranges between 2.5 and 5.9, EBFL (3.1-3.42), DBFL (1.5-1.94), MFL (1.81-2.1), CSL (1.7-1.97), OSL (2.05-2.42), WSL (2.4-3.6), SL (3.55-4.01), GL (4.5-5.12), PWL (3.52-4.62), CL (3.7-4.11), BUL (4.5-5.7), NVM (2.23-2.8), BL (3.8-4.02), and WB (6.82-7.16).

Table V: Change in Temperature and Standard Deviation for Different Land Use Land Cover

	Mean Temperature in Degree Celsius									
	2001		2006		2011		2016		2022	
Type of LULC class	Average	St.D	Average	St.D	Average	St.D	Average	St.D	Average	St.D
ENFL	20.8	2.5	21.45	5.9	18.3	2.6	18.3	2.93	19.14	2.5
EBFL	23	3.42	22.6	3.4	23.3	3.25	23.4	3.3	22.72	3.1
DBFL	30.1	1.94	28.84	1.64	29.44	1.6	29.56	1.55	28.3	1.5
MFL	27	2.1	27.03	1.8	27.31	1.81	26.62	1.96	26.21	1.9
CSL	33.9	1.93	32.6	1.97	34.53	1.72	34.31	1.7	34.8	1.7
OSL	39.9	2.42	38.4	2.31	39.25	2.05	39.9	2.33	39	2.2
WSL	23.1	3.6	22.96	3.1	23.9	2.9	23.9	2.85	23.6	2.4
SL	29.8	4.01	29.24	3.9	29.9	3.7	29.86	3.87	29	3.55
GL	35.4	5.12	34.2	4.8	35.1	4.51	35.6	4.73	35	4.5
PWL	27.14	4.5	26.6	3.93	26.42	3.52	27.65	4.62	26.7	3.83
CL	32.17	4.11	31.2	4.02	31.8	3.8	31.7	4.1	31.17	3.7
BUL	34.66	5.7	33.15	4.92	34.22	4.82	33.93	4.7	33.61	4.5
NVM	26.33	2.8	25.4	2.23	26.1	2.4	25.86	2.8	25.63	2.7
BL	45.54	4.02	44.15	4	43.95	3.9	45.1	3.95	43.92	3.8
WB	25.8	7.16	25.5	7.1	25.55	6.95	25.84	7.2	25.1	6.82

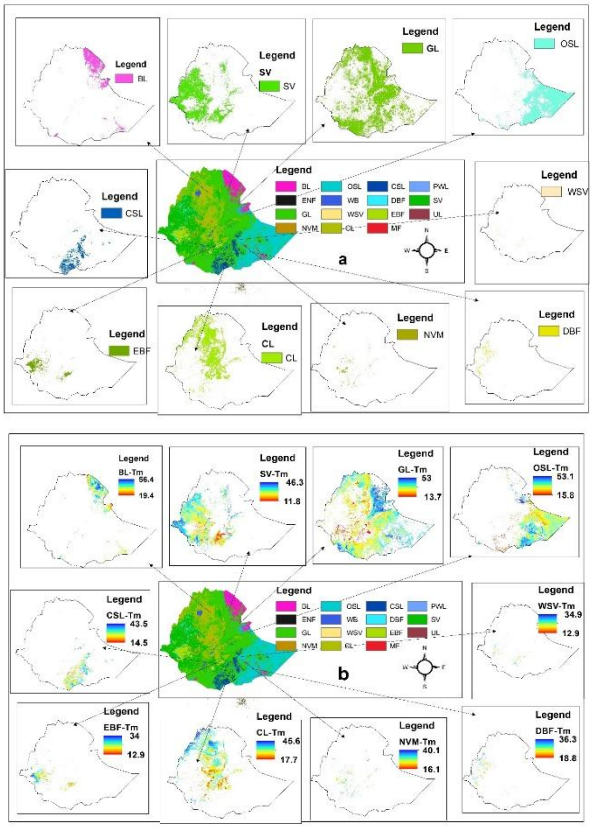

[Fig.6: Spatial Distribution of LULC(a) Crospondig with its LST(b) in 2022]

IV. DISCUSSION

By integrating Geographic Information Systems (GIS) and Remote Sensing (RS) techniques, this study systematically examined temporal and spatial changes in land use/land cover (LULC) and corresponding land surface temperature (LST) dynamics. Based on the characteristics of the study area and the dominance of specific land cover types, fifteen distinct LULC classes were identified and mapped. The final classified products provide a comprehensive representation of the principal land cover patterns and their spatial distribution across Ethiopia over the period 2002–2022. Classification accuracy was evaluated through a rigorous validation procedure using 500 randomly selected reference pixels, which were compared against ground-truth and independently derived LULC information for the corresponding time periods. The accuracy assessment results indicate that both overall accuracy and Kappa coefficient values for all LULC classes were within acceptable and reliable ranges across the selected years (2001, 2006, 2011, 2016, and 2022), as presented in Table I. These results confirm the robustness and reliability of the classified outputs for subsequent spatio-temporal analysis of LULC and LST dynamics. The Kappa coefficient is a statistical measure that quantifies the proportional improvement of a classification model over a random assignment of classes, thereby providing a robust assessment of agreement beyond chance. In contrast, user's accuracy represents the probability that a classified pixel corresponds correctly to its actual ground reference, while producer's accuracy indicates the extent to which real-world land cover categories are correctly represented in the classified output. The observed improvement in classification accuracy over time can be attributed to the increasing availability of higher-resolution and more detailed reference datasets in recent years, which enhances the reliability of validation procedures. Similar remote sensing-based classification and post-classification comparison approaches have been widely applied. As shown in Table II, the total area and proportional coverage of each LULC class were quantified relative to the overall landscape. Throughout the study period, grassland emerged as the dominant land cover type, accounting for approximately 36.53% to 44.75% of the total area, followed by savanna, which occupied between 15.92% and 17.56%. In contrast, evergreen needle-leaf forest represented the least extensive LULC class, consistently accounting for a negligible proportion of the landscape (≤ 0.0014%). A detailed breakdown of temporal LULC variations is provided in Table II. Change detection analysis was conducted through the classification of image pairs from two distinct temporal phases using a cross-tabulation (post-classification comparison) approach. This method enabled a systematic assessment of both the qualitative transitions between land use/land cover (LULC) classes and the quantitative magnitude of change across the period 2001–2022. The results reveal substantial spatial and temporal

variability in LULC dynamics throughout the study area. Overall, pronounced increases and decreases in specific LULC categories were observed over the study period, indicating significant landscape reorganisation. These changes are primarily driven by anthropogenic activities, particularly agricultural expansion, urbanisation, industrial development, and associated land conversion processes. Given that the majority of the study area is inhabited by rural populations whose livelihoods depend primarily on subsistence and small-scale agriculture, land transformation processes are closely linked to agricultural intensification and expansion. At the same time, urban growth remains comparatively limited yet locally significant. Population growth has led to the progressive subdivision of agricultural land through intergenerational inheritance, whereby farmland is continuously partitioned among offspring. This process has resulted in increasing land fragmentation and a concomitant decline in average farm size over time. Such structural changes have intensified pressure on natural resources, contributing to resource scarcity and accelerating environmental degradation within the study area. In parallel, rapid urban expansion driven by ongoing economic development in Ethiopia has significantly transformed existing land-use systems, with the increasing conversion of agricultural and other land-cover types into built-up areas. Furthermore, population pressure has stimulated the expansion of cultivated land, often at the expense of natural vegetation and grazing lands, thereby altering ecosystem structure and functionality. These findings are consistent with a growing body of literature from other regions of Ethiopia that identifies population growth as a primary driver of land-use/land-cover (LULC) change. Overall, both formal and informal human activities are the dominant forces driving LULC dynamics in the study area, a pattern that closely aligns with previous empirical studies [44]. Overall, the principal drivers of land use/land cover (LULC) change in the study area are multifaceted and include population pressure; the expansion of agriculture and settlements into marginal and mountainous terrains; increasing demand for fuelwood, construction timber, and agricultural implements; and charcoal production and intensive livestock grazing. These interacting pressures collectively contribute to accelerated landscape transformation and environmental degradation. In addition, landform characteristics strongly influence the spatial distribution and diversity of LULC patterns. Topographic variables such as elevation, slope, and aspect significantly regulate local microclimatic conditions by modifying the availability of heat and moisture and influencing soil physical and chemical properties. These factors, in turn, shape vegetation distribution and land-use suitability, thereby driving spatial heterogeneity in LULC, consistent with findings from previous studies [45, 46]. Similarly, climate change exerts both direct and indirect influences on LULC dynamics and ecosystem functioning by altering land-use practices, vegetation patterns, and the spatial distribution of ecological systems, as reported in the related literature. The mean Normalised Difference Vegetation Index (NDVI) values for the study area were 0.32 in 2001, 0.29 in 2006, 0.30 in 2011, 0.34 in 2016, and 0.32 in 2022. These values reflect temporal variability in vegetation health, greenness, biomass, and ecosystem condition. Additionally, land surface temperature (LST) across different land use and land cover (LULC) categories was systematically assessed over the study period. The results indicate pronounced thermal variability among land cover types, with the highest temperature recorded over barren land at 55.64 °C in 2016, and the lowest in evergreen broad-leaf forest (EBFL) at 10.1 °C in 2001. These extremes underscore the strong influence of surface characteristics on thermal regimes. Overall, the maximum mean LULC change over the past 22 years in Ethiopia was derived through a comparative analysis of LULC classes, identifying both the most and least dynamic land-cover transitions across spatial scales. The classification framework was developed by integrating supervised classification outputs with MODIS-derived datasets, revealing a heterogeneous landscape comprising diverse land-use and land-cover types. The observed variability in both LULC and LST is largely attributable to anthropogenic activities, which are themselves closely linked to the availability and management of water resources. Changes in land cover significantly influence local and regional temperature regimes, which in turn affect precipitation patterns, exacerbate water scarcity, and increase the frequency and severity of drought conditions. These interconnected processes ultimately have direct implications for the country's sustainable economic development.

V. CONCLUSION

This study evaluates land-use and land-cover dynamics in relation to land surface temperature using multi-temporal Landsat imagery. Significant differences are identified across land uses, and temperature variation is also detected within a single land-use/land-cover type. For each LULC classification, an accuracy assessment was calculated from 2001 to 2022, and the results demonstrate that user accuracy ranged from 95.6% to 98.4%. The producer accuracy of the LULC classification ranges from 93.8% to 98.2%, indicating well-classified LULC maps and being within the range for further analysis. The kappa coefficient values ranged from 0.86 to 0.95. The classification accuracy assessment met the criterion for land-use/land-cover classification. As a result, the classified images are valid for evaluating LULC change dynamics in the study area. The maximum likelihood algorithm for supervised classification of MODIS and Landsat images was applied using dominant LULC classes. The study area is classified as evergreen needle-leaf forests (ENFL), evergreen broad-leaf forests (EBFL), deciduous broad-leaf forests (DBFL), mixed forests (MFL), closed shrublands (CSL), open shrublands (OSL), woody savannas (WSL), savannas (SL), grasslands (GL), permanent wetlands (PWL), croplands (CL), urban and built-up lands (BUL), natural vegetation mosaics (NVM), barren (BL) and water bodies (WB). Based on the results obtained, the dominant LULC was grassland, covering 36.53-44.75% during the study period. In contrast, evergreen needle-leaf forest land use/land cover was the lowest, with an area coverage of less than or equal to 0.0014%. The evaluated mean NDVI values for the study area were 0.32 in 2001, 0.29 in 2006, 0.3 in 2011, 0.34 in 2016, and 0.32 in 2022, which are

characteristic of vegetation. The land surface temperature for the study area was also evaluated, and the mean spatial distribution of the study area LST ranges from 11.8 to 56.4°C in 2001, from 10.1 to 53.8°C in 2006, from 12.7 to 53.9°C in 2011, from 11.8 to 55.6°C in 2016, and from 12.2 to 53.7°C in 2022. The land surface temperature for each land-use/land-cover type was evaluated, and the highest temperature was observed in barren land at 55.64°C in 2016, whereas the lowest was observed in EBFL at 10.1 °C in 2001. The standard deviation of land surface temperature for ENFL ranges between 2.5 and 5.9, EBFL (3.1-3.42), DBFL (1.5-1.94), MFL (1.81-2.1), CSL (1.7-1.97), OSL (2.05-2.42), WSL (2.4-3.6), SL (3.55-4.01), GL (4.5-5.12), PWL (3.52-4.62), CL (3.7-4.11), BUL (4.5-5.7), NVM (2.23-2.8), BL (3.8-4.02), and WB (6.82-7.16).

The findings of this study provide substantial and policy-relevant insights for decision-makers and planning authorities. In particular, the results enable a critical evaluation of the effectiveness of existing land-use policies and support anticipation of future environmental and socio-economic challenges. This, in turn, facilitates the development of targeted and context-specific land management strategies.

Moreover, integrating spatially explicit future scenarios enhances evidence-based decision-making, promoting sustainable development, efficient natural resource management, and long-term socio-economic growth. In the context of climate change, anticipated alterations in precipitation regimes, temperature patterns, and other climatic variables are expected to exert significant pressure on land systems. Accordingly, land use and land cover (LULC) analysis provides a crucial framework for assessing the potential impacts of climate variability and change on land systems.

Such assessments are essential for understanding how shifts in temperature and rainfall may influence agricultural productivity, vegetation distribution, and water resource availability, thereby enabling policymakers to design appropriate adaptation and mitigation strategies. Furthermore, LULC analysis serves as a key tool for detecting environmental change and assessing associated ecological impacts. Projected land cover transitions, including deforestation and agricultural expansion, can be used to evaluate potential consequences for biodiversity, ecosystem integrity, and the sustainability of natural resources.

This knowledge is particularly important for supporting conservation planning, land-use zoning, protection of ecologically sensitive areas, and sustainable water resource management. In addition, the analysis of LULC dynamics and their associated risks provides critical inputs for disaster risk reduction. By identifying areas susceptible to floods, landslides, and other hydro-meteorological hazards, relevant agencies can strengthen early warning systems, improve land-use regulations, and enhance disaster preparedness and response planning.

ACKNOWLEDGEMENT

As the author of the manuscript “Spatiotemporal detection of land use/land cover (LULC) and land surface temperature (LST) using Landsat and MODIS data in Ethiopia, East Africa,” my declaration of interest is stated below by Agegnehu Kitanbo Yoshe. Arba Minch University, Arba Minch, Ethiopia

DECLARATION STATEMENT

I must verify the accuracy of the following information as the article's author.

- **Conflicts of Interest/ Competing Interests:** Based on my understanding, this article has no conflicts of interest.
- **Funding Support:** This article has not been funded by any organizations or agencies. This independence ensures that the research is conducted objectively and without external influence.
- **Ethical Approval and Consent to Participate:** The content of this article does not necessitate ethical approval or consent to participate with supporting documentation.
- **Data Access Statement and Material Availability:** The MODIS LULC dataset utilised was accessed on 25 July 2024 and available at https://lpdaac.usgs.gov/products/mcd12q1v061/ (Friedl & Sulla-Menashe, 2022). The MODIS Land Surface Temperature and Emissivity (MOD11) was accessed on 25 July 2024 and available at https://modis.gsfc.nasa.gov/data/dataprod/mod11.php (Wan et al., 2004).
- **Author’s Contributions:** Conceptualization, methodology, original draft writing, preparation, and development of the model were carried out by Agegnehu Kitanbo Yoshe.

REFERENCE

1. Ayele, A., Tarekegn, K. (2020). The impact of urbanisation expansion on agricultural land in Ethiopia: A review. *Environ. Socio-Econ. Stud. 8*, 73–80. DOI: https://doi.org/10.2478/environ-2020-0024
2. Samal, D.R., Gedam, S. (2021). Assessing the Impacts of Land Use and Land Cover Change on Water Resources in the Upper Bhima River Basin, India. *Environ. Chall. 5*, 100251. DOI: https://doi.org/10.1016/j.envc.2021.100251
3. Calicioglu, O., Flammini, A., Bracco, S., Bellù, L., Sims, R. (2019). The Future Challenges of Food and Agriculture: An Integrated Analysis of Trends and Solutions. *Sustainability* 11, 222. DOI: https://doi.org/10.3390/su11010222
4. Zabihi, M., Moradi, H., Gholamalifard, M., Khaledi Darvishan, A., Fürst, C. (2020). Landscape Management through Change Processes Monitoring in Iran—Sustainability *12*, 1753. DOI: https://doi.org/10.3390/su12051753
5. Das, S., Sarkar, R. (2019). Predicting the land use and land cover change using Markov model: a catchment level analysis of the Bhagirathi-Hugli River, Spatial Inf. Res. 27 (2019) 439e452, DOI: https://doi.org/10.1007/s41324-019-00251-7.
6. Tan, J., Yu, D., Li, Q., Tan, X., Zhou, W. (2020). Spatial relationship between land-use/ land-cover change and land surface temperature in the Dongting Lake area, China, Sci. Rep. 10 (2020) 1e9, DOI: https://doi.org/10.1038/s41598-020-66168-6.
7. Zoungrana, B.J.B., Conrad, C., Amekudzi, L.K., Thiel, M., Da, E.D., Forkuor, G., Low, F. (2015). Multi-temporal Landsat images and ancillary data for land-use/land-cover change (LULCC) detection in southwestern Burkina Faso, West Africa, Rem. Sens. 7 (2015) 12076e12102, DOI: https://doi.org/10.3390/rs70912076.
8. Cai, M., Ren, C., Xu, Y., Lau, K.K.L., Wang, R. (2018). Investigating the relationship between local climate zone and land surface temperature using an improved WUDAPT methodology - a case study of the Yangtze River Delta, China, Urban Clim. 24 (2018) 485e502,

DOI: https://doi.org/10.1016/j.uclim.2017.05.010.
9. Khan, M.S., Ullah, S., Sun, T., Rehman, A.U., Chen, L. (2020). Land-use/land-cover changes and their contribution to urban heat Island: a case study of Islamabad, Pakistan, Sustainability 12 (2020), DOI: https://doi.org/10.3390/su12093861
10. Ayele, G.T., Tebeje, A.K., Demissie, S.S., Belete, M.A., Jemberrie, M.A., Teshome, W.M., Mengistu, D.T., Teshale, E.Z. (2018). Time-series land-cover mapping and change-detection analysis using a geographic information system and remote sensing, Northern Ethiopia, Air Soil. Water Res. 11 (2018), DOI: https://doi.org/10.1177/1178622117751603.
11. Mondal, I., Thakur, S., Ghosh, P., De, T.K., Bandyopadhyay, J. (2019). Land Use/Land Cover Modelling of Sagar Island, India Using Remote Sensing and GIS Techniques, Springer Singapore, DOI: https://doi.org/10.1007/978-981-13-1951-8_69.
12. Thakur, S., Maity, D., Mondal, I., Basumatary, G., Ghosh, P.B., Das, P., De, T.K. (2021). Assessment of Changes in Land Use, Land Cover, and Land Surface Temperature in the Mangrove Forest of Sundarbans, Northeast Coast of India, Environ. Dev. Sustain. 23 (2021) 1917e1943, DOI: https://doi.org/10.1007/s10668-020-00656-7.
13. Saleem, M.S., Ahmad, S.R., Shafiq-Ur-Rehman, Javed, M.A. (2020). Impact assessment of urban development patterns on land surface temperature using remote sensing techniques: a case study of Lahore, Faisalabad, and Multan districts, Environ. Sci. Pollut. Control Ser. 27 (2020) 39865e39878, DOI: https://doi.org/10.1007/s11356-020-10050-5.
14. Pepin, N., Deng, H., Zhang, H., Zhang, F., Kang, S., Yao, T. (2019). An Examination of temperature trends at high Elevations across the Tibetan plateau: the use of MODIS LST to understand patterns of Elevation-Dependent Warming, J. Geophys. Res. Atmos. 124 (2019) 5738e5756, DOI: https://doi.org/10.1029/2018JD029798.
15. Prakash, S., Norouzi, H. (2020). Land surface temperature variability across India: a remote sensing satellite perspective, Theor. Appl. Climatol. 139 (2020) 773e784, DOI: https://doi.org/10.1007/s00704-019-03010-8.
16. John, J., Bindu, G., Srimuruganandam, B., Wadhwa, A., Rajan, P. (2020). Land use/land cover and land surface temperature analysis in Wayanad district, India, using satellite imagery, Spatial Sci. 26 (2020) 343e360, DOI: https://doi.org/10.1080/19475683.2020.1733662.
17. Bayissa, Y., Tadesse, T., Demisse, G., & Shiferaw, A. (2017). Evaluation of Satellite-Based Rainfall Estimates and Application to Monitor Meteorological Drought for the Upper Blue Nile Basin, Ethiopia. *Remote Sensing*, *9*(7), 669. DOI: https://doi.org/10.3390/rs9070669
18. Lemma, E., Upadhyaya, S., and Ramsankaran, R. (2022). Meteorological drought monitoring across the main river basins of Ethiopia using satellite rainfall products. *Environmental Systems Research*, 2–15. DOI: http://doi.org/10.1186/s40068-022-00251-x.
19. Yoshe, A.K. (2024). Water availability identification from GRACE dataset and GLDAS hydrological model over data-scarce river basins of Ethiopia, Hydrological Sciences Journal, 69:6, 721-745, DOI: http://doi.org/10.1080/02626667.2024.2333852
20. Ramachandran, R.M., Reddy, C.S. (2017). Monitoring of deforestation and land-use changes (1925–2012) in Idukki district, Kerala, India, using remote sensing and GIS, J. Indian Soc. Remote Sens. 45 (1) 163–170, DOI: https://doi.org/10.1007/s12524-015-0521-x.
21. Basukala, A.K., Oldenburg, C., Schellberg, J., Sultanov, M., Dubovyk, O. (2017). Towards improved land use mapping of irrigated croplands: performance assessment of different image classification algorithms and approaches, Eur. J. Remote Sens. 50 (1) 187–201, DOI: https://doi.org/10.1080/22797254.2017.1308235
22. Dibaba, W.T., Demissie, T.A., Miegel, K. (2020). Drivers and Implications of Land Use/Land Cover Dynamics in Finchaa Catchment, Northwestern Ethiopia. *Land*, *9*, 113. DOI: https://doi.org/10.3390/land9040113
23. Minta, M., Kibret, K., Thorne, P., Nigussie, T., Nigatu, L. (2018). Land Use and Land Cover Dynamics in Dendi-Jeldu Hilly-Mountainous Areas in the Central Ethiopian Highlands. *Geoderma* 2018, *314*, 27–36. DOI: https://doi.org/10.1016/j.geoderma.2017.10.035
24. Yoshe, A.K. 2025. Land use land cover detections using MODIS MCD12Q1 V6.1 and ESRI Sentinel-2 datasets in the Lake Chamo catchment. H2Open Journal (2025) 8 (1): 20–41, DOI: https://doi.org/10.2166/h2oj.2024.038.
25. Srivastava, A., Kumari, N. & Maza, M. (2020) Hydrological response to agricultural land use heterogeneity using variable infiltration capacity model, Water Resour. Manag., 34, 3779–3794. DOI: https://doi.org/10.1007/s11269-020-02630-4
26. Yesuph, A. Y. & Dagnew, A. B. (2019). Land Use/Cover spatiotemporal dynamics, driving forces, and implications in the Beshillo catchment of the Blue Nile basin, northeastern highlands of Ethiopia, Environ. Syst. Res., 8, 21. DOI: https://doi.org/10.1186/s40068-019-0148-y
27. Li, X., Zhou, Y., Asrar, G.R., Zhu, Z. (2018). Creating a seamless 1 km resolution daily land surface temperature dataset for urban and surrounding areas in the conterminous United States, Remote Sens. Environ. 206 (2018) 84e97, DOI: https://doi.org/10.1016/j.rse.2017.12.010.
28. Mal, S., Rani, S., Maharana, P. (2021). Estimation of spatio-temporal variability in land surface temperature over the Ganga River Basin using MODIS data. Estimation of spatio-temporal variability in land surface temperature over the Ganga River Basin using MODIS data, Geocarto Int. 1e23, DOI: https://doi.org/10.1080/10106049.2020.1869331.
29. Aliani, H., Malmir, M., Sourodi, M., Kafaky, S.B. (2019). Change detection and prediction of urban land-use changes using the CA–Markov model (case study: Talesh County). *Environ. Earth Sci. 78*, 546. DOI: https://doi.org/10.1007/s12665-019-8557-9
30. da Cunha, E.R., Santos, C.A.G., da Silva, R.M., Bacani, V.M., Teodoro, P.E., Panachuki, E., de Souza Oliveira, N. (2020). Mapping LULC types in the Cerrado-Atlantic Forest ecotone region using a Landsat time series and object-based image approach: A case study of the Prata River Basin, Mato Grosso do Sul, Brazil. *Environ. Monit. Assess. 192*, 136. DOI: https://doi.org/10.1007/s10661-020-8093-9
31. Rimal, B., Zhang, L., Keshtkar, H., Haack, B.N., Rijal, S., Zhang, P. (2018). Land Use/Land Cover Dynamics and Modelling of Urban Land Expansion by the Integration of Cellular Automata and Markov Chain. *ISPRS Int. J. Geo-Inf. 7*, 154. DOI: https://doi.org/10.3390/ijgi7040154
32. Mirchooli, F., Mahboobeh Kiani-Harchegani, Abdulvahed Khaledi Darvishan, Samereh Falahatkar, Seyed Hamidreza Sadeghi, Spatial distribution dependency of soil organic carbon content to important environmental variables, Ecological Indicators, Volume 116, 2020, 106473, DOI: https://doi.org/10.1016/j.ecolind.2020.106473.
33. Chen, X., and Zhang, Y. (2017). "Impacts of Urban Surface Characteristics on Spatiotemporal Pattern of Land Surface Temperature in Kunming, China."Sustainable Cities and Society 32: 87–99. DOI: http://doi.org/10.1016/j.scs.2017.03.013.
34. Guha, S., and H. Govil. (2021). "An Assessment on the Relationship between Land Surface Temperature and Normalised Difference Vegetation Index." Environment, Development and Sustainability 23 (2): 1944–1963. DOI: http://doi.org/10.1007/s10668-020-00657-6
35. Roşca, C. F., Harpa, G. V., Croitoru, A. E., Herbel, I., Imbroane, A. M. and Burada, D. C. (2017). "The Impact of Climatic and Non-climatic Factors on Land Surface Temperature in Southwestern Romania." Theoretical and Applied Climatology 130: 775–790. DOI: http://doi.org/10.1007/s00704-016-1923-6.
36. Ali, J. M., Marsh, S. H. and Smith, M. J. (2017). "A Comparison between London and Baghdad Surface Urban Heat Islands and Possible Engineering Mitigation Solutions."Sustainable Cities and Society 29: 159–168. DOI: http://doi.org/10.1016/j.scs.2016.12.010.
37. Madanian, M., Soffianian, A. R., Koupai, S. S., Pourmanafi, S., and Momeni, M. (2018). "The Study of Thermal Pattern Changes Using Landsat-derived Land Surface Temperature in the Central Part of Isfahan Province." Sustainable Cities and Society 39: 650–661. DOI: http://doi.org/10.1016/j.scs.2018.03.018.
38. Pal, S., and Ziaul, S. (2017). "Detection of Land Use and Land Cover Change and Land Surface Temperature in EnglishBazar Urban Centre." The Egyptian Journal of Remote Sensing and Space Sciences 20: 125–145. DOI: http://doi.org/10.1016/j.ejrs.2016.11.003.
39. Zhang, F., Kung, H., Johnson, V. C., LaGrone, B. I. andWang, J.(2017). "Change Detection of Land Surface Temperature (LST) and Some Related Parameters Using Landsat Image: A Case Study of the Ebinur Lake Watershed, Xinjiang, China." Wetlands 1–16. DOI: http://doi.org/10.1007/s13157-017-0957-6.
40. Tayyebi, A., H. Shafizadeh-Moghadam, and Tayyebi, A. H. (2018). "Analysing Long-term Spatio-temporal Patterns of Land Surface Temperature in Response to Rapid Urbanisation in the Mega-city of Tehran." Land Use Policy 71: 459–469. S. H. SADEGHI ET AL. DOI: https://doi.org/10.1016/j.landusepol.2017.11.023.14
41. Jafari, R., and Hasheminasab, S. (2017). "Assessing the Effects ofDam Building on Land Degradation in Central Iran with Landsat LST and LULC Time Series." Environmental Monitoring and Assessment 189: 74. DOI: http://doi.org/10.1007/s10661-017-5792-y.
42. Tan, J., Yu, D., Li, Q., Tan, X.and Zhou, W. (2020). "Spatial Relationship between Land-use/land-cover Change and Land Surface Temperature in the Dongting Lake Area, China." Scientific Reports 10 (1): 1–9. DOI: http://doi.org/10.1038/s41598-019-56847-4.
43. Mustafa, E. K., Liu, G., El-Hamid, A., Hazem, T. and Kaloop, M. R. (2021). "Simulation of Land Use

Published By:
Blue Eyes Intelligence Engineering and Sciences Publication (BEIESP)

Dynamics and Impact on Land Surface Temperature Using Satellite Data." GeoJournal 86 (3):1089–1107.
DOI: http://doi.org/10.1007/s10708-019-10115-0.
44. Monteiro, L., Sentelhas, P. & Pedraa, G. U. (2018) Assessment of NASA/POWER satellite-based weather system for Brazilian conditions and its impact on sugarcane yield simulation, Int. J. Climatol., 38, 1571–1581. DOI: https://doi.org/10.1002/joc.5282
45. Hoylman, Z. H., Jencso, K. G., Hu, J., Martin, J. T., Holden, Z. A., Seielstad, C. A., & Rowell, E. M. (2018). Hillslope topography mediates spatial patterns of ecosystem sensitivity to climate, J. Geophys. Res.: Biogeosci., 123, 353–371.
DOI: https://doi.org/10. 1002/2017JG004108.
46. Chen, X., Jiang, L., Zhang, G., Meng, L., Pan, Z., Lun, F., & An, P. (2021). Green-depressing cropping system: a referential land use practice for fallow to ensure a harmonious human-land relationship in the farming-pastoral ecotone of northern China, Land Use Policy, 100, 104917. DOI: https://doi.org/10.1016/j.landusepol.2020.104917.
47. Guo, Y., Fang, G., Xu, Y. P., Tian, X. & Xie, J. (2020). Identifying how future climate and land use/cover changes impact streamflow in Xinanjiang Basin, East China. Sci. Total Environ., 710 (2020), Article 136275. DOI: https://doi.org/10.1016/j.scitotenv.2019.136275

AUTHOR'S PROFILE

Dr. Eng. Sci. Agegnehu Kitanbo Yoshe is a researcher and lecturer at the Water Technology Institute, Faculty of Water Resources and Irrigation Engineering, Arba Minch University, Ethiopia. He holds a BSc in Irrigation and Water Resources Engineering from Hawassa University, an MSc in Irrigation and Drainage Engineering from Arba Minch University, a PhD from Irkutsk National Research Technical University, Russia, and a D.Sc. in Hydrogeology from Tomsk Polytechnic University, Russia. His research focuses on groundwater and surface water hydrology, climate change impacts, ecohydrology, hydraulic engineering, sustainable water management, and applications of artificial intelligence. He integrates remote sensing, GIS, and multi-criteria decision analysis to support groundwater development and water resources management.